Structural Monitoring and Maintenance, *Vol. 11, No. 4 (2024) 263-275*
https://doi.org/10.12989/smm.2024.11.4.263

Evaluation of embedded FBG sensors for strain monitoring of residential timber buildings under various wind speeds

Abolghassem Zabihollah*[1], Poorya Hajyalikhani[2a] and Rajesh Vuddandam[1b]

[1]*Department of Mechanical, Environmental, and Civil Engineering, Tarleton state University, Stephenville, USA*
[2]*Department of Engineering Technology, Tarleton state University, Stephenville, USA*

(*Received June 28, 2024, Revised August 3, 2024, Accepted August 8, 2024*)

Abstract. This study explores the use of Fiber Bragg grating (FBG) systems as embedded sensors for monitoring strain and temperature in residential timber buildings. FBG sensors are chosen for their corrosion resistance, immunity to electromagnetic interference, and high sensitivity. They have been successfully employed as embedded sensors for real-time structural health monitoring in aerospace, automotive, and civil infrastructure applications. A proof-of-concept experimental setup has validated the system's performance and functionality. Multiple one-story and two-story scaled-down (~1:20) prototype timber buildings were constructed and placed in a wind tunnel to assess their structural performance and stability under wind speeds ranging from 0 to 150 mph. FBG sensors attached to the buildings measured strain and wavelength changes in real-time. The measured strain data can be used to estimate the load-carrying capacity and assess the building's reliability. The FBG sensors demonstrated accurate measurement and real-time monitoring of strain changes in selected structural elements during high wind speeds. Assessment results can inform condition-based maintenance, safety evaluations, and stability reports. Additionally, the system can issue real-time warnings for potential failures and damages, thereby enhancing the overall resilience of residential buildings.

Keywords: condition-based; FBG; health monitoring; hurricane; residential building, stability

1. Introduction

Annually, strong winds, hurricanes, and tornadoes inflict significant damage and claim lives in coastal regions, prompting researchers in the structural health monitoring (SHM) community to develop cost-effective monitoring systems for residential buildings. While civil infrastructure like bridges and tunnels, as well as critical buildings such as hospitals and high-rises, have benefited from SHM systems for a decade, these systems remain prohibitively expensive for residential use.

An SHM system typically includes an array of sensors, a signal processing unit, and a communication platform for timely reporting and issuing evacuation or maintenance recommendations. Reports generated by the monitoring system are utilized by local authorities, construction firms, insurance providers, and real estate agents to assess the structure's safety and

*Corresponding author, Associate Professor, E-mail: azabihollah@tarleton.edu
[a]Ph.D., E-mail: hajyalikhani@tarleton.edu
[b]Ph.D., E-mail: vuddandam@tarleton.edu

http://www.techno-press.org/?journal=smm&subpage=7 ISSN: 2288-6605 (Print), 2288-6613 (Online)

reliability, enabling appropriate actions to safeguard residents' lives.

Perhaps the occurrence of hurricanes is the most common weather condition issues leading to catastrophic damages in residential buildings particularly in coastal areas (Landsea 2016).

A hurricane arises from atmospheric turbulence, generating high winds (90-135 mph) that exert strong forces on structures. Traditionally, mitigating hurricane damage involves hardening homes (Milnes and Twisdale 2008). However, devising effective hardening or mitigation strategies requires assessing structural performance and health conditions. Accurate estimation of potential losses is crucial for implementing condition-based mitigation efforts to reduce future losses. Numerous studies have been conducted to estimate hurricane damage across various types of structures (Amirinia 2017). A critical aspect in predicting damage from future hurricanes is the development and accumulation of micro-damage resulting from multiple hurricane events.

This phenomenon can gradually weaken the structure, potentially leading to sudden failure even under forces lower than intended. Current evaluation methods for residential buildings primarily rely on visual inspection due to their affordability and simplicity. However, the accuracy of visual inspection is heavily reliant on the inspector's experience, making it susceptible to human errors. Moreover, visual inspections are conducted periodically and do not offer continuous information about the building's condition between inspections.

The SHM system comprises sensors, data acquisition and transmission systems, and a database for efficient data management and health diagnosis, including damage detection, safety evaluation, and reliability analysis. Over the past two decades, significant research has focused on enhancing the accuracy and functionality of each component of SHM systems (Abdulkarem *et. al.* 2020).

SHM technology plays a crucial role in evaluating the safety and durability of structures during and after hurricanes, ensuring their continued serviceability and sustainability (Farrar and Worden 2007). By offering precise and real-time damage assessment, SHM helps prevent catastrophic damage, provides early disaster warnings, and ultimately saves lives during environmental disasters like hurricanes. Most of SHM techniques used for structural health monitoring of buildings use global SHM strategies in which the dynamic response of the building under local ambient dynamic forces is estimated (Frangopol and Messervey 2009). However, global SHM techniques may not provide accurate location of weak elements in the building. Therefore, a local SHM strategy is required for monitoring individual structural components, such as columns, walls, roof, etc. Local SHM techniques rely on measurement of influencing element wise parameters including strain and displacement (Chen 2018).

Structural Health Monitoring (SHM) systems applied to civil infrastructures such as bridges and high-rise buildings involve monitoring the structure by assessing its performance during operation.

Sivasuriyan *et al.* (2021) investigated the use of accelerometers for operational monitoring and damage evaluation of multi-story buildings. SHM techniques has also been used for monitoring special building such as historic buildings (Barsocchia *et al.* 2020).

Most of the existing SHM systems use electrical sensors, including strain gauges, piezoelectric, and linear variable differential transformers (LVDTs). Piezoelectric sensors are relatively low-cost sensors that provide sufficient accuracy to be used in residential buildings.

Marveas and Bartzanas (2021) conducted a review on the application of various sensor types and technologies for structural health monitoring of agricultural structures. Park and Inman (2006) explored the use of piezoelectric sensors for detecting damage in buildings through impedance measurements. The effectiveness of piezoelectric sensors in SHM depends significantly on their placement within the structure, necessitating optimization algorithms to determine sensor count

and optimal locations (Wieslaw and Malinowski 2019).

Dziadak (2020) used metal strain gauges to measure the strain on the main roof girders of the building. The measured strain is then transmitted to the processing unit wireless communication network.

More recently, Fiber Bragg Grating (FBG) sensors have gained prominence in SHM systems for civil infrastructure, including dams and high-rise buildings. Braunfelds *et. al.* (2021) investigated the application of FBG sensors for monitoring the structural integrity of road asphalt. Sliti and Boudriga (2021) utilized FBG sensors for vibration monitoring of buildings, particularly for assessing structural performance during earthquakes.

Amaya and Sierra-Perez (2022) employed embedded FBG sensors to monitor the structural health of reinforced concrete structures. They utilized wavelength changes as indicators to monitor structural integrity variations caused by different excitation frequencies. Recently, Wu *et. al*. (2022) summarized the contemporary applications of fiber optic sensors for structural health monitoring in buildings.

This paper aims to present a cost-effective and efficient Structural Health Monitoring (SHM) system for residential buildings. It explores the feasibility of using FBG sensors to monitor strain and ensure the structural integrity of residential timber buildings under wind loads and hurricanes. An analytical approach employing a frame element with 3 degrees of freedom per node was used to assess the frame's response to wind pressure. Additionally, a proof-of-concept experiment was conducted using an in-house experimental setup. One-story and two-story scaled-down prototypes of timber buildings were constructed and tested in a wind tunnel to evaluate the effectiveness of FBG sensors in monitoring the structural health of residential buildings.

2. Modeling building with embedded FBG sensors

2.1 Dynamic modeling of timber building

For a planar frame element shown in Fig. 1, there are 3 degrees of freedom (DOFs) at each node in the local coordinate system.

The DOFs of a frame element are the axial deformation in the x direction, u, deflection in the y direction, v, and the rotation in the x–y plane and concerning the z-axis, θ_z. Therefore, a frame element with two nodes has a total of 6 DOFs. The dynamic response of a frame is given as

$$[M]\{\ddot{d}\} + [D]\{\dot{d}\} + [K]\{d\} = \{F(t)\} \tag{1}$$

where $F(t)$, d, M, and K are the applied force vector, displacement vector, mass matrix, and stiffness matrix, respectively. Matrix D represents the structural damping and can be determined as:

$$[D] = \alpha[K] + \beta[M] \tag{2}$$

where α and β are related to the critical damping of the first two modes of vibration. For example, α = 0.2 and β =0.005.

The element matrices of the frame element composed of axial and flexural components as

$$[K] = \begin{bmatrix} [K_{axial}] & 0 \\ 0 & [K_{flexural}] \end{bmatrix} \tag{3}$$

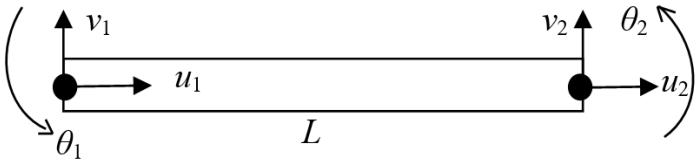

Fig. 1 A FEM frame element

$$[M] = \begin{bmatrix} [M_{axial}] & 0 \\ 0 & [M_{flexural}] \end{bmatrix} \tag{4}$$

where the axial and flexural components are defined as

$$[K_{axial}] = \begin{bmatrix} \frac{AE}{L} & -\frac{AE}{L} \\ -\frac{AE}{L} & \frac{AE}{L} \end{bmatrix} \tag{5}$$

$$[M_{axial}] = \frac{\rho AL}{420}\begin{bmatrix} 140 & 70 \\ 70 & 140 \end{bmatrix} \tag{6}$$

The flexural components are given as

$$[K_{flexural}] = \frac{EI}{L}\begin{bmatrix} \frac{12}{L^2} & \frac{6}{L} & \frac{-12}{L^2} & \frac{6}{L} \\ \frac{6}{L} & 4 & \frac{6}{L} & 2 \\ & & \frac{12}{L^2} & -\frac{6}{L} \\ sym & & & 4 \end{bmatrix} \tag{7}$$

$$[M_{flexural}] = \frac{\rho AL}{420}\begin{bmatrix} 156 & 22L & 54 & -13L \\ & 4L^2 & 13L & -3L^2 \\ & & 140 & -22L \\ sym & & & 4L^2 \end{bmatrix} \tag{8}$$

where A, E, I, and ρ indicate cross section area of the element, young's modulus of the element's material, the moment of inertia about z axis, and the material density, respectively.

The transpose of vector of displacement $\{d\}^T$ composed of axial and flexural deformation as

$$\{d\}^T = \{d_{axial} \quad d_{flexural}\} \tag{9}$$

where

$$\{d_{axial}\} = \{u_1 \quad u_2\}, \qquad \{d_{flexural}\} = \{v_1 \quad \theta_{z1} \quad v_1 \quad \theta_{z2}\} \tag{10}$$

Having the nodal flexural displacement in the element, the flexural deformation of the element is determined as

$$v(x) = [N]\{d_{flexural}\} \tag{11}$$

where $[N]$ is the vector of shape functions determining the flexural deformation of the element which, considering Euler Bernoulli beam theory, is given as

$$N(1) = 1 - \frac{3x^2}{L^2} + \frac{2x^3}{L^3}, N(2) = x - \frac{2x^2}{L} + \frac{x^3}{L^2}, N(3) = \frac{3x^2}{L^2} - \frac{2x^3}{L^3}, N(4) = \frac{x^3}{L^2} - \frac{x^2}{L} \quad (12)$$

where y_{max} is the maximum distance from the neutral axis of the element.

Using the displacement vector, the strain along an element is determined as

$$\varepsilon_x(x) = -y_{max} \frac{d^2[N]}{dx^2} \{d_{flexural}\} \quad (13)$$

For more details one may consults the book written by Reddy (Reddy 2005).

The force vector $F(t)$ is determined considering the pressure induced due to wind velocity. Wind pressure depends on wind speed, surrounding terrain including topography, and probabilities of directionality and occurrence of wind speed (ASCE 7-10). For the sake of simplicity, the pressure of wind is given by

$$P_{wind} = C_p \left(\frac{1}{2} \rho_{air} V_{wind}^2\right) \quad (14)$$

2.2 Strain measurement using FBG sensors

The principle of a FBG sensor is based on the wavelength shifting of the reflected spectrum when strain or temperature change arises in the element. FBG sensors provide advantages such as multi and continuous sensing using only a single fiber line, ease of placing and embedding in the structure, electromagnetic interference immunity, high sensitivity, and multiplexing capability. Temperature and strain variations applied to the gratings cause shift in their Bragg wavelengths as

$$\Delta\lambda_i = k_{Ti}\Delta T + k_{\varepsilon i}\Delta\varepsilon \quad (15)$$

where, k_{Ti} and $k_{\varepsilon i}$ are thermal sensitivity and strain sensitivity of FBG sensors. Considering a constant temperature of the structure during testing, the induced strain on the element can be estimated as:

$$\Delta\varepsilon = \frac{\Delta\lambda_i}{k_{\varepsilon i}} \quad (16)$$

For more details on modeling FBG for strain measurement, one may consult article written by Sarkandi and Zabihollah (2011).

3. Experimental works

To illustrate the performance and functionality of the proposed system, a proof-of-the-concept system consisting of a simplified wooden frame has been built. The performance of the attached FBG sensors on measuring the strain has been studied experimental works as explained in the following subsections.

3.1 Building prototype

According to (ASCE 7-10) (Sliti and Boudriga 2021), residential building models scaled for wind tunnel testing typically range up to 1:50. Given typical heights of 4 meters for one-story (with a ceiling height of 3.75 meters) and 7.5 meters for two-story buildings, the prototypes in this

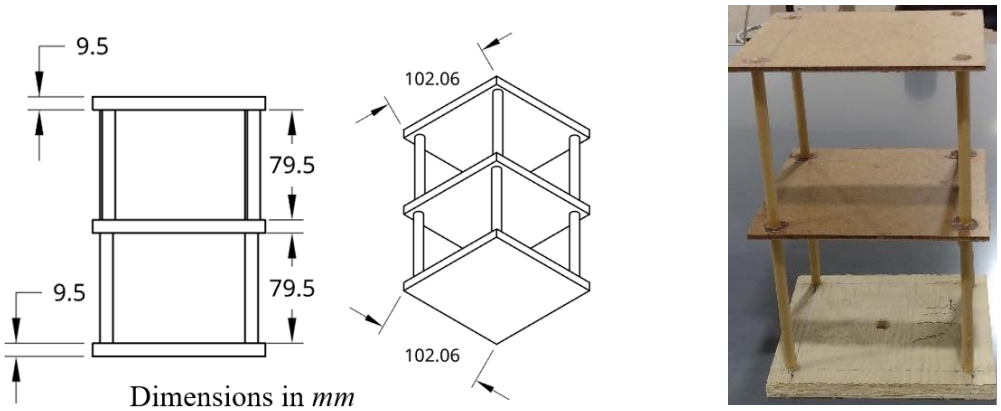

(a) Geometrical drawing (b) Built prototype

Fig. 2 Two-story sample, (a) schematic and (b) prototype

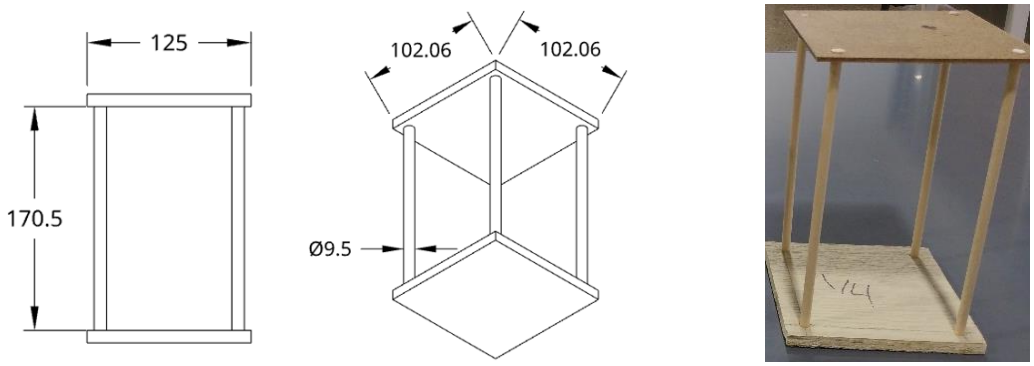

(a) Geometrical drawing (b) Built prototype

Fig. 3 One-story (high ceiling), (a) schematic, (b) prototype

study are scaled at 1:20. Figs. 2 and 3 illustrate the geometric and constructed models of the one-story and two-story frame specimens. These frames are constructed from pine wood with a Young's modulus of elasticity of 9 GPa.

3.2 Modal testing of the prototype

Understanding the dynamic properties of buildings is crucial due to vibrations induced by hurricanes. The prototype timber buildings detailed in Section (3.1) were utilized to ascertain their resonance frequencies. Using a Hammer Impact (EMA-02-C16), a modal analyzer (S20-P02), and vibration analyzer software from Crystal Instruments®, the natural frequencies of both the one-story and two-story prototype buildings were determined. The test procedure is illustrated in Fig. 4.

The modal testing results include the first three natural frequencies, along with their corresponding amplitudes and damping coefficients, extracted from the resonance frequency report generated by the software. Table 1 presents these parameters for both the one-story and two-story buildings.

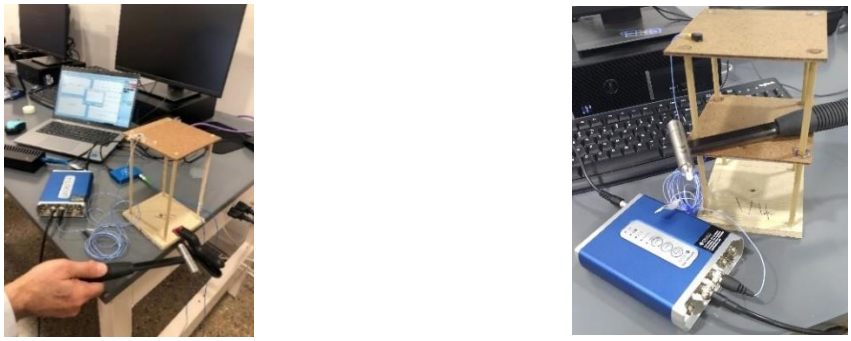

(a) one-story (b) two-story

Fig. 4 Modal testing of the prototype buildings (a) one-story (high ceiling) and (b) two-story

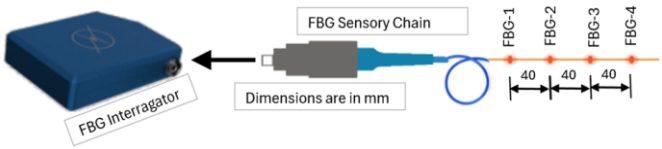

Fig. 5 Schematic illustration of fiber optic FBG sensor (a) FBG-MR0010 and (b) FBGX100 Interrogator

Table 1 Modal testing of frames

	Mode (*Hz*)			Amplitude (m/s^2/*N*)			Damping Coefficient		
	1	2	3	1	2	3	1	2	3
one-story	30.47	34.37	37.50	158.22	149.84	127.71	0.051	0.034	0.037
two-story	25.78	32.81	35.93	264.22	165.82	127.39	0.030	0.028	0.060

The results of modal testing have been verified by writing a finite element code in MATLAB based on Eqs. (3) and (4). It is worth noting that the natural frequencies of the frame structure are the square roots of the eigenvalues of the global stiffness and mass matrices. In the present work, for the sake of brevity, a two-dimensional one-story frame has been considered with the same geometries (Fig. 3(a)) and material properties described in Section 3.1. The fundamental frequency of the two-dimensional frame has been determined as 38 Hz.

3.3 Measuring strain using FBG

A bare fiber optic cable (FBG-MR0010, purchased from Micronor Sensors, Inc.) composed of four FBG sensors located at 40 mm apart as shown in Fig. 5 is used to determine the induced strain on the selected element of the frame.

The fiber optic cable is linked to an FBGX100 Interrogator (from FISENS®). FBG sensors are affixed to the outer surface of the front wall (facing the wind force) using adhesive tape, as depicted in Fig. 6. For brevity and given that structural modeling and stress analysis of such a basic structure are routine for structural engineers, specific details of the stress analysis are omitted here.

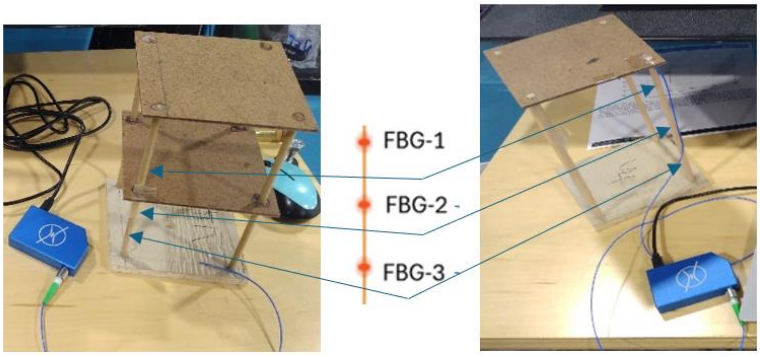

(a) (b)

Fig. 6 Connecting FBG sensors to (a) one-story and (b) two-story buildings

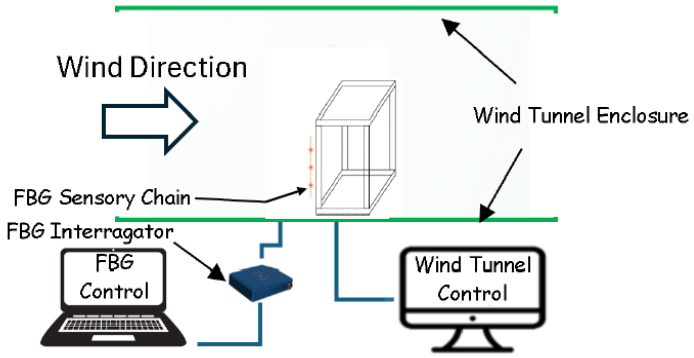

Fig. 7 Schematic illustration of wind tunnel testing

3.4 Wind tunnel testing

To simulate the strong winds and hurricanes in the laboratory, a wind tunnel made by (aerolab®) has been used.

The wind speed is controlled by varying the fan speed (RPM). The relationship between the fan speed and the wind speed in the testing area is extracted from the calibration data provided by (aerolab®) as:

$$\textit{Wind speed (mph)} = 0.062\ \textit{Fan (RPM)}$$

The test setup includes a wind tunnel with speed controlled by adjusting the fan speed via a computer. The strain measured by FBG sensors is collected by an FBG interrogator, which transmits the optical signals to a computer for visualization. Fig. 7 provides a schematic diagram of the test setup, which includes the building prototype, wind tunnel chamber, wind speed controller, FBG interrogator, and computer for visualizing the induced strain.

The one-story and two-story prototype buildings were placed in the wind tunnel, as shown in Figs. 7 and 8. FBG sensors were connected to the FBG interrogator to measure the induced strain on the prototype buildings under varying wind speeds.

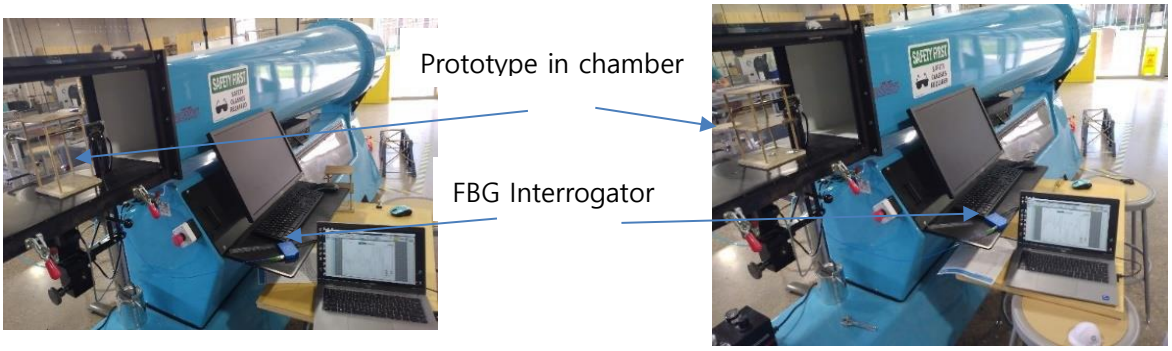

(a) one-story (b) two-story

Fig. 8 Strain measurement of the frames in wind tunnel, (a) one-story and (b) two-story

Table 2 strain (μm/m) at the selected locations for one-story building (Fig. 3)

FBG	Wind speed, mph						
Location, mm	20	40	60	80	100	120	140
5	0.82	3.29	7.40	13.16	20.56	29.60	40.30
45	0.79	3.18	7.16	12.72	19.87	28.62	38.95
85	0.71	2.85	6.41	11.40	17.82	25.66	34.92

Table 3 strain (μm/m) at the selected locations for two-story building (Fig. 2)

FBG	Wind speed, mph						
Location, mm	20	40	60	80	100	120	140
5	0.2	0.82	1.85	3.28	5.14	7.40	10.07
45	0.19	0.79	1.78	3.18	4.96	7.15	9.37
85	0.17	0.71	1.60	2.85	4.45	6.41	8.73

4. Results and discussions

4.1 Numerical strains

The induced strains at three different points along the column of the one-story building shown in Fig. 6b have been determined at various wind speeds. Table 2 provides the induced strains at these locations for different wind speeds. As expected, the induced strains at all three points increase with higher wind speeds, due to the increased wind pressure as determined by Eq. (11). The maximum strain occurs at the FBG sensor located 5 mm from the fixed support. The trend shows that strain increases up to 5 mm, then begins to decrease, which is due to the boundary conditions of a typical column.

Similarly, Table 3 presents the induced strains at various locations under different wind speeds for the two-story building prototype. As anticipated, the results for the two-story building prototype are consistent with those observed in the one-story building prototype.

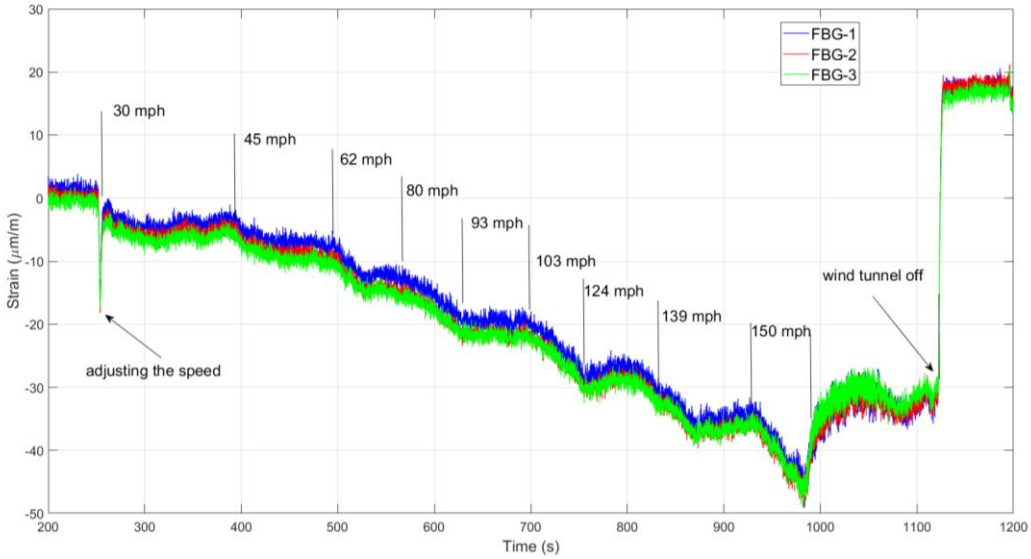

Fig. 9 Strain measured by FBG sensors of a one-story frame at different wind speed

4.2 Experimental results

To demonstrate the performance and functionality of the building integrated with FBG sensors, the one-story structure with attached FBG sensors, as shown in Fig. 8(b), was placed in a wind tunnel and subjected to various wind speeds. The wind speed was adjusted by controlling the fan's speed, as described in Eq. (14), ranging from 0 mph to 150 mph.

Fig. 9 displays the response of the FBG sensors at different wind speeds. As observed, FBG 3 shows the highest value as it is located near the fixed support, as shown in Fig. 6(b). FBG 1 shows the lowest value since it is positioned close to the ceiling support. A sharp increase in strains can be seen at 250 seconds, which occurred at the start of the test when the operator mistakenly increased the wind speed. Another notable point is around 900 seconds, where the strain begins to gradually increase from approximately -50 μm/m to -30 μm/m, coinciding with the operator gradually reducing the fan speed. At 1150 seconds, the wind tunnel was shut down, causing the strain to sharply decrease. At this point, the strain passes zero and continues to rise to a positive value of about 15 μm/m, indicating the column's vibrating behavior under sudden load changes.

It is noted that the strains computed using FEM procedure are approximately 20% lower than the strain measured by FBG sensors. This is due to considering perfect support conditions at end nodes of the column. For example, all degrees of freedom at the fixed support are considered zeros while in prototype model, the fixing condition is not perfect.

To visualize the functionality of the strains measured by the FBG sensors at different wind speeds, the wind test is repeated for different wind ranges assuming the wind continues at a specific speed for a given time before changing to the next level. Fig. 10 shows the performance of FBG 1 at different wind speed ranges. One may realize a sharp drop at the wind range of 10-20 mph. This is due to an operator mistake when trying to adjust the fan speed. On the other hand, this is an indication of capability of the FBG to measure and record the strain in real-time. Furthermore, it is observed that by increasing the wind speed, the induced strain increases.

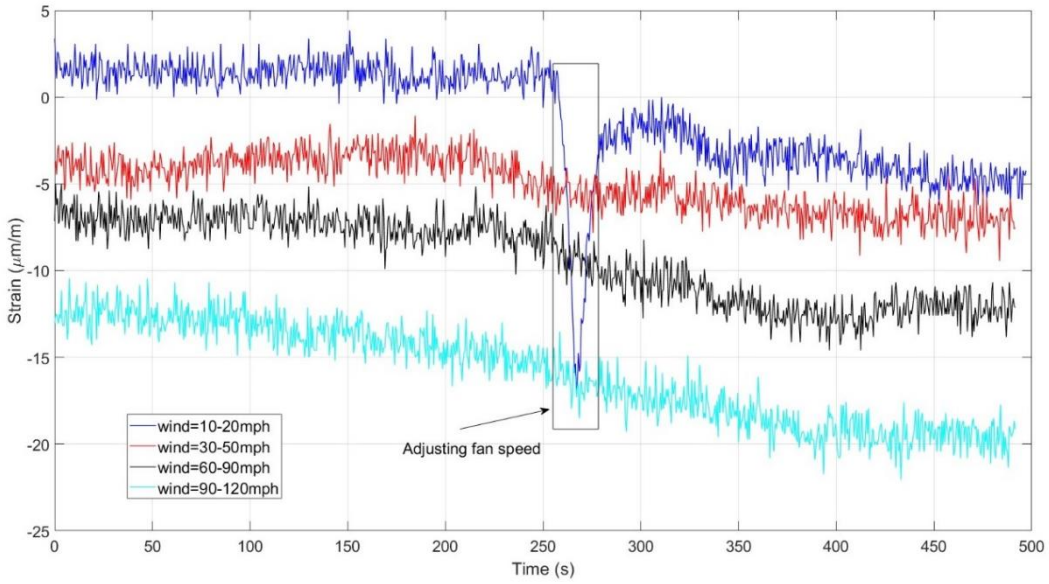

Fig. 10 Strain measured by FBG sensors one-story frame at different ranges of wind speed

Similarly, the induced strains at the column, depicted in Fig. 6(a), were measured using FBG sensors attached at specific points shown in the same figure, under varying wind speeds from 0 mph to 130 mph. Fig. 11 illustrates the time response of the FBG sensors to different wind speeds for the two-story prototype shown in Fig. 6(a). The wind speed change test protocol was designed to evaluate the performance of the monitoring system under varying wind speeds and directions.

Furthermore, FBG 2 exhibits the highest value because it is located near the fixed support of the first roof, as shown in Fig. 6(a). The observed strain trend is influenced by the boundary conditions applied to the column. A particularly noteworthy aspect of the results is the FBG sensor's ability to accurately detect changes in strain in real-time.

However, it was realized that the strain measured by FBG sensors are about 20% lower than that of the numerical values determined from finite element model. This is because the FEM results are determined by assuming recorded material properties of the wood and theoretical boundary conditions for end nodes while experimental.

5. Conclusions

The use of Fiber Bragg Grating (FBG) sensors for monitoring the structural integrity of residential timber buildings has been studied. Numerical results of induced strain at selected columns under varying wind speeds were determined using a two-dimensional frame element model. Two wooden frames, designed and built to simulate timber buildings, were placed in a wind tunnel and subjected to wind speeds ranging from 0-150 mph for a one-story frame and 0-130 mph for a two-story frame.

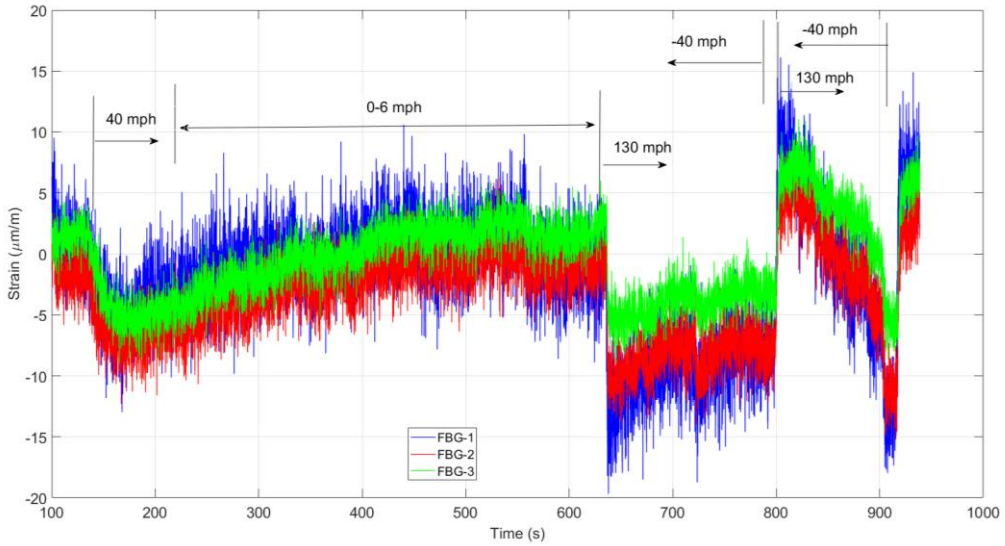

Fig. 11 Strain measured by FBG sensors two-story frame at different wind speed and directions

Additionally, modal testing was conducted to examine the building's dynamic behavior. The monitoring system's performance was validated under both gradual and randomly changing wind speed conditions. This research concludes that:

- Surface mounted FBG sensors accurately measure the induced strains due to wind load in real-time.
- The effectiveness and accuracy of the FBG are affected by the wind speeds for a common range of hurricanes (0-150mph).
- The results demonstrate the potential of embedded FBG sensors as a low-cost, accurate monitoring system for the structural health of residential buildings during hurricanes.
- The strain measured by FBG sensors at different speeds and for various buildings generates a database for machine learning and artificial intelligence algorithms.
- The measured strain data can be used to estimate the load-carrying capacity and assess the building's reliability, safety evaluations, and stability reports.
- The system can issue real-time warnings for potential failures and damages, thereby enhancing the overall resilience of residential buildings.

Future work will focus on developing and implementing signal processing algorithms to estimate a building’s structural reliability as well as generating a condition-based maintenance strategy.

Acknowledgments

Authors wish to thank the support provided by Mayfield College of Engineering at Tarleton State University.

References

Abdulkarem, M., Samsudin, K., Rokhani, F. and Rasid, M. (2020), "Wireless sensor network for structural health monitoring: A contemporary review of technologies, challenges, and future direction", *Struct. Health Monit.*, **19**(3), 693-735. https://doi.org/10.1177/1475921719854528.

Amaya, A. and Sierra-Pérez, J. (2022), "Toward a structural health monitoring methodology for concrete structures under dynamic loads using embedded FBG sensors and strain mapping techniques", *Sensors.*, **22**, 4569. https://doi.org/10.3390/s22124569.

Amirinia, G. and Jung, S. (2017), "Buffeting response analysis of offshore wind turbines subjected to hurricanes", *Ocean Eng*., **141**(3), 1-17. https://doi.org/10.1016/j.oceaneng.2017.06.005.

Barsocchi, P., Bartoli, G., Betti, M., Girardi, M., Mammolito, S., Pellegrini, D. and Zini, G. (2020), "Wireless sensor networks for continuous structural health monitoring of historic masonry towers", *Int. J. Archit Herit*., **15**(1), 22-44. https://doi.org/10.1080/15583058.2020.1719229.

Braunfelds, J., Ugis, S., Peteris, S., Rims, J., Toms, S., Dmitrii, R., Ilya, L., Jurgis, P., Sandis, S., Viktors, H., and Vjaceslavs, B. (2021), "FBG-based sensing for structural health monitoring of road infrastructure", *J. Sensors*, 8850368, 11 pages. https://doi.org/10.1155/2021/8850368.

Chen, H.P. (2018), *Structural health monitoring of large civil engineering structures*, (1st Ed.), Oxford: John Wiley & Sons.

Dziadak, B. (2020), "Structural health monitoring system for snow and wind load measurement", *Electron.*, **9**(4), 609. https://doi.org/10.3390/electronics9040609.

Farrar, C.R. and Worden, K. (2007), "An introduction to structural health monitoring", *Philos. Transact. A Math. Phys. Eng. Sci.*, **365**, 303-315. https://doi.org/10.1098/rsta.2006.1928.

Frangopol, D.M. and Messervey, T.B. (2009), *Maintenance Principle for Civil Structures*. John Wiley & Sons, Chichester, UK.

Landsea, C. (2016), "How many direct hits by hurricanes of various categories have affected each state", Atlantic Oceanographic and Meteorological Laboratory, https://www.aoml.noaa.gov/hrd/Landsea/deadly/

Maraveas, C. and Bartzanas, T. (2021), "Sensors for structural health monitoring of agricultural structures", *Sensors.*, **21**, 314. https://doi.org/10.3390/s21010314.

Mehta, K.C. and Coulbourne, W.L. (2010), *Wind loads: guide to the wind load provisions of ASCE 7-10*, Published by American Society of Civil Engineers.

Milnes, M.C. and Twidale, L. (2008), "2008 Florida residential wind loss mitigation study", Final Report 18401; Applied Research Associates Inc, https://www.floir.com/sitedocuments/aralossmitigationstudy.pdf

Park, G. and Inman, D. (2006), "Structural health monitoring using piezoelectric impedance measurements", *Philos. Transact. A Math. Phys. Eng. Sci.*, **365**, 373-392. https://doi.org/10.1098/rsta.2006.1934.

Reddy, J.N. (2005), *An Introduction to the Finite Element Method*, (3rd Edi., McGraw Hill.

Sarkandi, Gh. and Zabihollah, A. (2011), "A computational model for health monitoring of storage tanks using fiber Bragg grating optical fiber", *J. Civ. Struct. Health Monit.*, **1**, 97-101. https://doi.org/10.1007/s13349-011-0010-z.

Sivasuriyan, A., Vijayan, D.S., Gorski, W., Wodzynski, L., Vaverkova, M.D. and Koda, E. (2021), "Practical implementation of structural health monitoring in multi-story buildings", *Buildings.*, **11**(6), 263. https://doi.org/10.3390/buildings11060263.

Sliti, M. and Boudriga, N. (2021), "Building structural health monitoring: An FBG-based estimation of external vibrations", *Proceedings of the 18th International Multi-Conference on Systems, Signals & Devices (SSD)*, 22-25, March 2021. https://doi.org/10.1109/SSD52085.2021.9429378.

Wieslaw O., Rohan S. and Malinowski, P. (2019), "Optimization of sensor placement for structural health monitoring: A review", *Struct. Health Monit.*, **18**(3), 963-988. https://doi.org/10.1177/1475921719825601.

Wu, T., Liu, G., Fu, S. and Xing, F. (2022), "Recent progress of fiber-optic sensors for the structural health monitoring of civil infrastructure", *Sensors.*, **20**, 4517. https://doi.org/10.3390/s20164517.

MK